Quasi-online flood forecasting downstream of dams based on rainfall thresholds

Bahram Saghafian, Saeed Golian and Hossein Khodadadi

ABSTRACT

Dams are built to supply water to users and often to protect people and properties against floods in downstream areas. Efficiency of dams for flood control is improved substantially if a flood forecasting system is implemented. Rainfall threshold (RT) depths correspond to the occurrence of critical discharge at given cross-sections for given rainfall durations and initial soil moisture conditions of the upstream watershed. Here, we present an RT-based approach for offline flood forecasting downstream of dams. The proposed methodology incorporates rainfall-runoff and reservoir routing models while the spatial distribution of rainfall is probabilistically modeled based on a Monte Carlo approach. The RT curves are derived as a function of initial water elevation in the reservoir. The algorithm is implemented for a flood-prone area downstream of a dam in southwestern Iran. The results showed a clear rise in the RT values compared to the no-dam case, which is mainly due to the reservoir routing effect. The rate of rise in the RT values decreased with higher initial water elevation in the reservoir. The proposed method also provides the operator with the flexibility of adopting one of the various RT curves subject to different probabilities based on risk tolerance.

Key words | Monte Carlo, neural network, rainfall threshold, real-time flood forecasting, reservoir water elevation

Bahram Saghafian
Hossein Khodadadi
Science and Research Branch,
Islamic Azad University,
Tehran,
Iran

Saeed Golian (corresponding author)
Civil Engineering Department,
Shahrood University of Technology,
Shahrood,
Iran
E-mail: *s.golian@shahroodut.ac.ir*

INTRODUCTION

Among all natural disasters worldwide, floods cause over one-third of the total estimated damages and about two-thirds of all people affected (UNEP 2002). Globally, the average number of flood victims for a 5-year period from 1973 to 1977 was 19 million while it increased substantially to 111 million over the 1988 to 1992 period and still further to 131 million over the 1993 to 1997 period. Approximately, 7,000 people have died annually worldwide over the last 25 years (Luino *et al.* 2012). In 1998 alone, the flood death toll came close to 30,000. In Iran, flood losses have risen by about 250% in the past 50 years (Vatanfada 2001). Karkheh basin is one of the most flood-prone regions in Iran. Table 1 contains loss-of-life figures as well as financial damages to different sectors in the basin.

The countermeasures to reduce the negative effects of flooding can be divided into structural and non-structural approaches. Financial and environmental consequences of structural methods may sometimes give priority to implementation of non-structural approaches. However, in some cases, a single flood control approach may not be sufficient. Conjunctive use of dams and flood forecasting systems representing a merger of structural and non-structural approaches must be quite effective for flood control in sensitive downstream areas. Because of its simplicity and flexibility, the rainfall threshold (RT) approach has become particularly popular in landslide and debris flow hazard forecasting (Neary & Swift 1987; Martelloni *et al.* 2012). In the context of flood forecasting, RT is defined as the cumulative rainfall depth, for a given initial soil moisture condition, which causes critical water level (or discharge) in a particular cross-section of the river, i.e., target point (Amadio *et al.* 2003; Martina *et al.* 2006; Ntelekos *et al.* 2006; Norbiato *et al.* 2008; Montesarchio *et al.* 2009; Golian *et al.* 2010,

doi: 10.2166/nh.2013.048

Table 1 | Flood damages reported between 1991 and 2005 in Karkheh river basin, Iran

Structural services and buildings	Stockbreeding and agriculture	Human losses
182 million dollars	93 million dollars	123 persons

2011). Threshold exceedance could cause the rainfall to produce flooding at the target point and trigger an alert in the flood warning systems (Georgakakos 1995). Golian *et al.* (2010) developed a Monte Carlo (MC) simulation approach to consider the uncertainty of rainfall spatial distribution in calculating the threshold values. They considered sub-watersheds' rainfall depth to be spatially independent and compared the results with historical events. Golian *et al.* (2011) later outlined the advantages of copula methods to model the spatial correlation between dimensionless sub-basin rainfalls in an RT-based flood forecasting system.

In none of the aforementioned studies have RTs been extracted for target points at the downstream of planned or constructed dams. This paper addresses the derivation of RT curves for a target point located at the downstream of a dam reservoir. The methodology incorporates artificial neural network (ANN) and storage indication methods for rainfall-runoff (R-R) modeling and reservoir routing, respectively. These two models were coupled in a Monte Carlo simulation framework to consider the uncertainty of rainfall spatial distribution. The proposed methodology was applied to the flood-prone sub-basin of Karkheh, in southwest Iran.

STUDY REGION

The study region is a part of the great Karkheh basin located in southwest Iran between 46°1′ and 49°1′ E longitude and 33°3′ and 34°58′ N latitude, spreading over the three provinces of Hamadan, Kermanshah, and Lorestan (Figure 1). The area of study sub-basin is approximately 19,904 km^2, with a mean watershed elevation of 1,744 masl (meters above sea level). In the presence of the Zagros mountains and a dominant Mediterranean climate, the area is subject to an average annual precipitation of 456 mm, mean annual temperature of 16.5 °C, and mean annual relative humidity of 55%. Kouranbozan dam is being built on the Seymareh River in

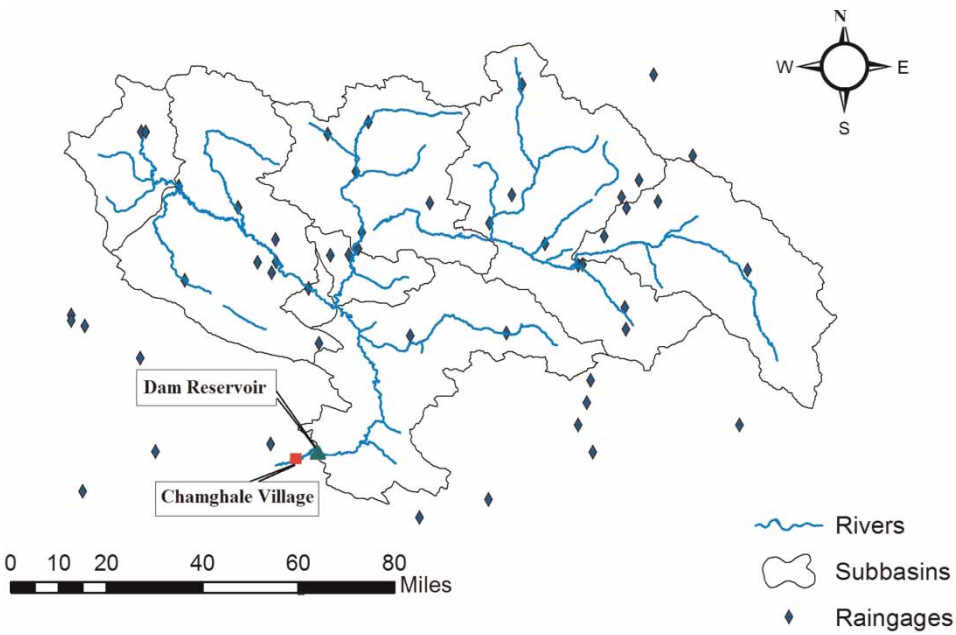

Figure 1 | Location of target point and Koranbouzan dam reservoir.

Lorestan province and is a rock fill dam. The average annual inflow to the dam reservoir is 76.2 m^3/s. The reservoir storage capacity is 4,002 MCM (million cubic meters) and the dam height above the foundation is 160 m. The Saymareh river forms at the confluence of the Gharasoo and Gamasiab rivers with an overall river length of 296.5 km. This mountainous basin was divided into eight sub-basins (Figure 1). Approximately 2 km downstream of the dam, a village, called Chamghale (35 km northeast of Kouhdasht city), is designated as the target point subject to flood hazard.

The study area is one of the most vulnerable flood-prone regions in Iran and requires protective measures. The historical statistics show that in the period of 1991–2005, 52 devastating floods occurred in this basin.

By analyzing the streamflow records, map of the floodplain land use, and topography of the target point, the critical flood was determined as 250 m^3/s, beyond which floods will cause hazardous damage to the residential zones.

METHODOLOGY

In this study, to derive RT values at the target point, an inverse modeling approach was adopted in which a system of coupled models was iteratively run with different rainfall depths for a specific set of rainfall duration, soil moisture condition, and initial reservoir water elevation. The coupled model is a combination of a calibrated R-R model to transform rainfall into runoff as well as a reservoir routing model to route flood hydrographs through the reservoir. In this research, an ANN was employed as a tool for R-R modeling and storage-indication (pulse) method for hydrologic routing of floods through the reservoir. The distance between the dam site and the downstream target point is rather short (<2 km). Thus, the effect of downstream river routing could be ignored. More details are presented in the next sections.

Rainfall temporal and spatial distribution

Available data consist of observed rainfall for 53 raingauges inside and around the basin in 6-hour time intervals for eight sub-basins and the corresponding inflow data to the dam reservoir. The Monte Carlo approach as used by Golian *et al.* (2010, 2011), was applied in this study to take into account the uncertainty of spatial distribution of rainfall. After derivation of rainfall maps of several historical events, dimensionless rainfall depths were calculated for each sub-basin by dividing the average rainfall values of that sub-basin with the average rainfall values of the whole basin. Inverse distance weighting (IDW) method was employed to derive spatial distribution of rainfall over the basin. Using Anderson–Darling goodness-of-fit test, best probability distribution function (PDF) was fitted to each sub-basin dimensionless rainfall values. Based on these PDFs, a set of 1,000 random dimensionless rainfalls were generated for each sub-basin. These values were reweighted to avoid bias as follows:

$$w_i' = w_i \times \frac{\sum_{j=1}^{N} A_j}{\sum_{j=1}^{N} A_j \cdot w_j} \tag{1}$$

where w_j' is the reweighted dimensionless rainfall, w_i is the initial dimensionless rainfall of the i-th sub-basin, A_i is the area of the i-th sub-basin and N is the number of sub-basins. After reweighting, the $\sum_{j=1}^{N} A_j \cdot w_j / \sum_{j=1}^{N} A_j = 1$ relationship is satisfied.

Now, derived dimensionless rainfall values (w_i) were multiplied by any assumed basin average rainfall amount ($\bar{P}$) to determine the average rainfall of each sub-basin. These values were transformed to hyetographs (distributed in time) according to the regional precipitation pattern (Figure 2), which is expressed as a relationship between percentage of rainfall depth and duration.

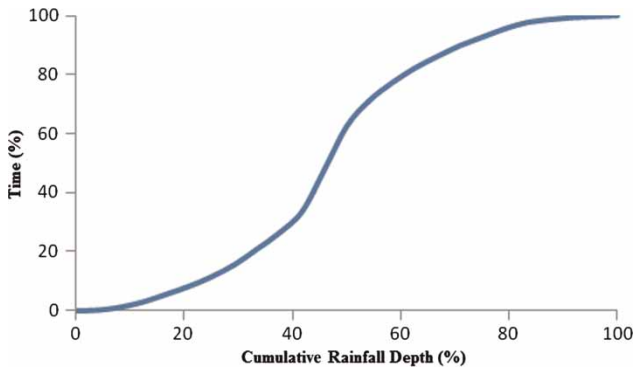

Figure 2 | Regional temporal rainfall pattern.

R-R modeling

R-R modeling is considered the most essential component in the flood estimation procedure. However, despite its importance, simulating the basin's response to rainfall remains a challenging issue due to its complex non-linear nature. In recent years, there has been a growing interest in application of soft computing methods, e.g., ANNs in hydrology (e.g., Rajurkar *et al.* 2002; Zhang & Govindaraju 2003; Wilby *et al.* 2003; Giustolisi & Laucelli 2005; Jain & Srinivasulu 2006; Saliha *et al.* 2011; Saghafian *et al.* 2013). ANN models remain relatively robust in the presence of noisy or missing inputs (Dawson & Wilby 1998), although many other studies have shown over-fitting problems in the presence of noisy data (Haykin 1999). Overall, ANNs are widely used as an effective tool for modeling non-linear, complicated R-R processes, especially when the underlying physical relationships are not fully understood.

Here, a multi-layer feed-forward neural network (MLFFNN) with back-propagation (BP) learning algorithm was employed to derive the inflow hydrograph to the dam reservoir. Numerous studies have reported simulation success by the MLFFNN trained by the standard BP algorithm (e.g., Rumelhart *et al.* 1986; Coulibaly 2000). The Levenberg-Marquardt method was selected as the BP learning algorithm, with linear transfer function (Purelin) and hyperbolic tangent sigmoid transfer function (tansig) as the transfer functions of the output and hidden layers, respectively. From all the data, 70% was used for training the ANN, 15% for validation, and the remainder (15%) for testing. Through trial-and-error, rainfall depths of two previous time steps ($P(t–1)$ and $P(t–2)$) were considered as inputs of the ANN. In addition, the effect of considering previous stage discharge ($Q(t–1)$) in simulating current discharge ($Q(t)$) was also examined (Figure 3).

Hall & Minns (1993) showed that antecedent rainfall intervals are highly dependent on the time of concentration of the drainage area, while outflow is a function of rainfall in previous or concurrent intervals. Time of concentration of the basin was determined as 16 hours through the application of the Bransby–Williams equation as follows:

$$t_c = \frac{21.3L}{A^{0.1}S^{0.2}} \tag{2}$$

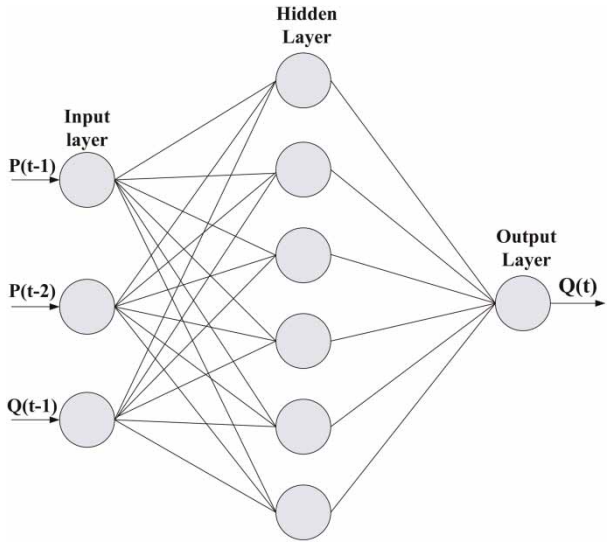

Figure 3 | Structure of the three-layer ANN in this study.

where S is the mean river slope (%), A is the basin area (km^2), and L is the main river length (km). Thus, antecedent rainfalls of say 16 hours (approximately three 6-hr time steps) could not influence the current runoff.

Reservoir routing

For hydrologic routing of floods through the reservoir, the 'storage-indication' or 'pulse' method was used (USBR 1974; Linsley *et al.* 1992). In this method, physical properties of the dam reservoir are embedded in a function which relates the storage (S) and outflow (O) variables. Parameter N is defined as a function of storage and discharge as follows:

$$N = \frac{S}{\Delta t} + \frac{O}{2} \tag{3}$$

S-O relationship was provided by the Iran Water and Power Resources Development (IWPRD) Company for the study reservoir (Table 1 in Appendix A, available online at http://www.iwaponline.com/nh/045/048.pdf). For each time step (6-hr), N is calculated as follows:

$$N_t = N_{t-1} + \frac{1}{2}(I_t + I_{t-1}) \tag{4}$$

where I represents the inflow discharge. Applying the S-O relationship, the outflow discharge in the present step (O_t) may be derived.

It is worth mentioning that a simple rule curve was considered for the study dam and no other management measures were involved in this regard.

Monte Carlo algorithm

MC algorithm involves the use of randomly generated samples for estimation of intractable procedures (e.g., R-R). MC is based on the law of large numbers such that the average of the results obtained from a large number of trials should be close to the historical records and will tend to become closer as more trials are conducted.

To derive RT values that correspond to a critical discharge at the target point (namely Chamghale village downstream of Koranbouzan reservoir in this study), an inverse modeling approach was adopted. The set of generated and subsequently reweighted dimensionless rainfall weights (w') were multiplied by the assumed (initial) basin's mean rainfall value ($\bar{P}$). Then, mean rainfall of each sub-basin was determined by ($P_i = P \times w'_i$) where i stands for sub-basin. The P_i values were transformed to hyetographs using a regionally dominant temporal pattern, i.e., Huff method in this case study, for a given rainfall duration (D). Using the trained ANN model, the inflow hydrograph to the reservoir was simulated and subsequently routed through the reservoir subject to a given initial water elevation. If the peak discharge at the target point (Q_{peak}) was within the critical discharge interval (critical discharge, Q_T, plus or minus 5%), the value of basin average rainfall ($\bar{P}$) would be labeled as the RT value corresponding to the rainfall duration of D. Otherwise, depending on whether the critical discharge was non-exceeded or exceeded, a rainfall fraction depth (ΔP) was added or subtracted from the previous basin average rainfall depth ($\bar{P}_{new} = \bar{P}_{old} \pm \Delta P$) and the above steps were repeated until a threshold value was obtained for the given set of dimensionless rainfall values. The number of iterations was set to 1,000 for each combination of examined rainfall durations (12, 18, 24, 30, 36, and 40 hours) and initial reservoir water elevations (1,020, 1,040, 1,080 masl, as well as the case without reservoir). The initial soil moisture condition was considered as dry (AMC I) as this is the dominant moisture condition in the region. Nevertheless, derivation of RT curves is possible via similar methodology. The flowchart of the proposed algorithm for RT extraction is shown in Figure 4.

Model evaluation

A number of criteria based on a contingency table were used to assess the accuracy of the proposed approach. Contingency tables are highly flexible and may be used to

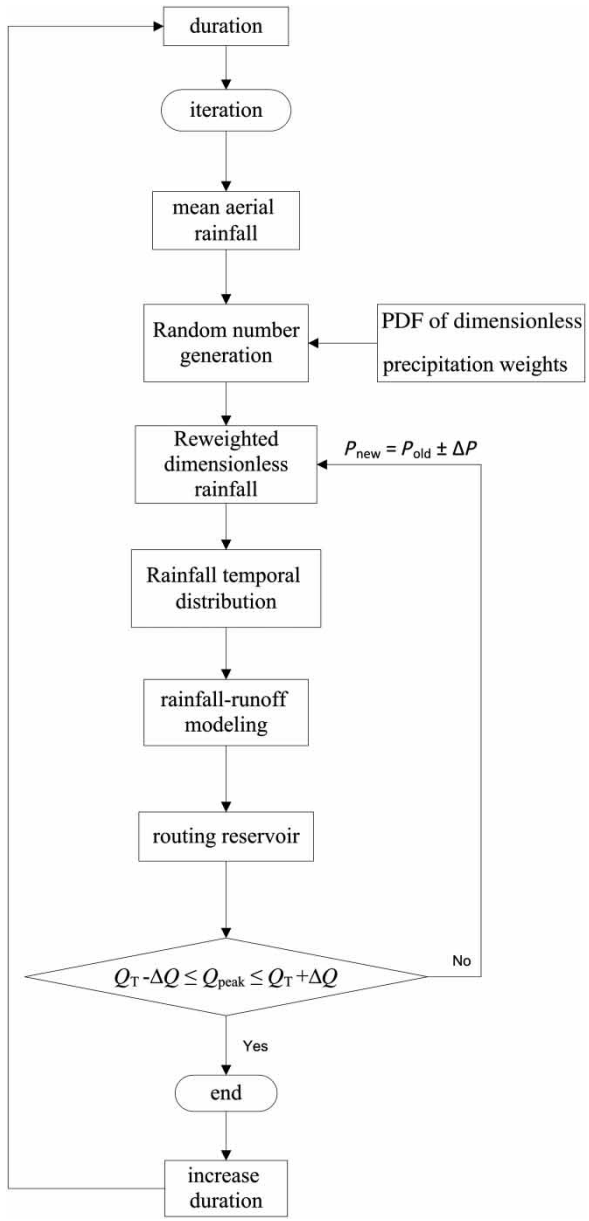

Figure 4 | Flowchart of RT extraction algorithm.

Table 2 | Forecast contingency table

	Forecast	
Observation	*Warning*	*No warning*
Event	Hit (h)	Miss (m)
Non event	False alarm (f)	Correct rejection (c)

estimate the quality of a deterministic forecasting system (Mason & Graham 1999). In their simplest form, a 2 by 2 table indicates the capability of the model to anticipate the occurrence of flood events (Table 2).

In the context of flood forecast, the following outcomes are possible: a hit, if a flood event occurs and a warning is issued; false alarm, if a flood event does not occur but a warning is issued; miss, if an event occurs but no warning is issued; correct rejection, if a flood event does not occur and a warning is not issued. The following three statistics may be used as a benchmark for model evaluation:

$$\text{Critical success index (CSI)} = \frac{h}{h+m+f} \tag{5}$$

$$\text{Hit rate (HR)} = \frac{h}{h+m} \tag{6}$$

$$\text{False rate (FR)} = \frac{f}{h+f} \tag{7}$$

All of the above statistics vary between 0 and 1. However, the upper range is desirable in CSI and HR while in the case of FR, the lower limit is preferred.

RESULTS AND DISCUSSION

In the developed ANN model, data were divided into training, validation, and testing sets. The ANN predictions were compared with the observed streamflows using a number of statistical indexes such as mean-square error (MSE) and the coefficient of determination (R^2) as follows:

$$\text{MSE} = \frac{\sum_{i=1}^{n} (x_i - \mu)^2}{n} \tag{8}$$

where x_i is the observed streamflow value (m^3/s) and μ is the mean of streamflow (m^3/s).

$$R^2 = \frac{SS_{\text{err}}}{SS_{\text{tot}}} \tag{9}$$

where SS_{err} is sum of the squares of residuals and SS_{tot} is the total sum of squares.

Five different ANN architectures with different inputs were examined in this study (Table 3 and Figure 3). In the hydrological modeling context, the input pattern consists of rainfall depths and discharges at previous time steps while the output is the discharges at the current time step.

As far as the number of hidden layers is concerned, there is no universal theory to determine the number of hidden layers and neurons a priori. This is usually conducted via a trial-and-error procedure. The comparison of the performance of a number of networks allowing different inputs led to the choice of the fourth model (Table 3) with six neurons in the hidden layer. Hall & Minns (1993) indicated that the number of effective antecedent rainfall

Table 3 | ANN models considered in the study and their performance statistics

		MSE (validation phase) $(m^3/s)^2$			R^2		
Inputs	**Neurons in hidden layer**	**Training**	**Validation**	**Test**	**Training**	**Validation**	**Test**
$P(t-1)$, $P(t-2)$	9	0.183	0.212	0.292	0.517	0.456	0.367
$P(t-1)$, $P(t-2)$	5	0.164	0.172	0.195	0.692	0.589	0.518
$P(t-1)$, $P(t-2)$, $P(t-3)$	11	0.157	0.166	0.189	0.822	0.683	0.588
$P(t-1)$, $P(t-2)$, $Q(t-1)$	6	0.102	0.121	0.134	0.973	0.867	0.765
$P(t-1)$, $P(t-2)$, $P(t-3)$, $Q(t-1)$	5	0.117	0.134	0.157	0.931	0.820	0.724

where t = present time, P = basin average rainfall depth, and Q = discharge.

ordinates (on discharge of current time step) is broadly related to the lag time of the drainage area. Here, the concentration time is about 16 hours which is slightly less than three 6-hr time steps; hence, inputs for up to three previous time steps were examined (i.e., $P(t)$, $P(t-1)$, $P(t-2)$, and $P(t-3)$). Results also showed that adding $Q(t-1)$ as an input decreases the mean square error of the network by almost 31% and increases the R^2 by 47% in the test phase. Comparison of the observed and simulated discharges in the validation and test phases shows good agreement.

The scatter plot of observed and simulated flows gives a clear indication of the simulation capability of the developed model for a wide range of flows (Figure 5).

For each rainfall duration and reservoir initial water level, the RT values were first sorted. On the basis of Weibull probability, rainfall depths corresponding to 10, 50, and 90% probabilities of occurrence were extracted. Figure 6 shows the RT curves with different probabilities corresponding to initial water elevation of 1,040 m in the dam reservoir.

Based on the CSI criterion, which represents a comprehensive indicator of the success of the forecasting system in comparison with FR and HR criteria (Norbiato *et al.* 2009), the 90% RT curve was found to perform better compared to other curves (Figure 7). Hence, for all initial water elevation scenarios, the 90% probability curve was selected for further analyses. Figure 8 quantitatively demonstrates, as expected,

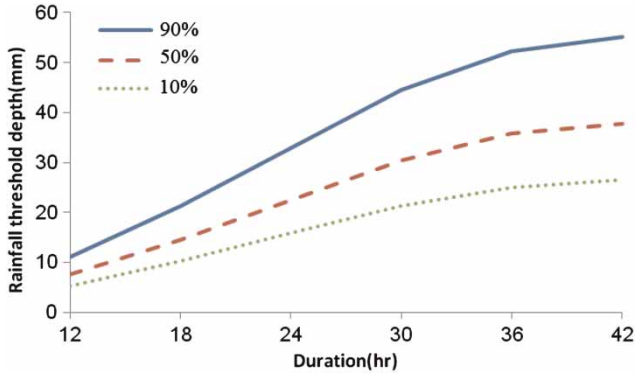

Figure 6 | RTs with different probabilities corresponding to reservoir water elevation of 1,040 m.

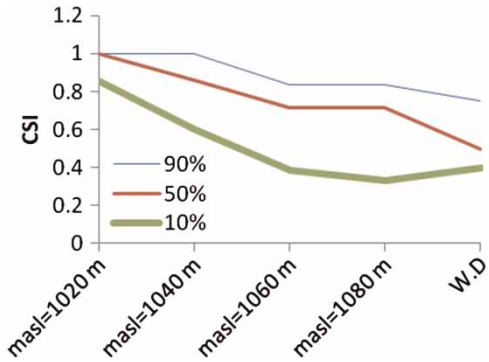

Figure 7 | Critical success index (CSI) for 10, 50, and 90% RT curves as a function of reservoir initial water elevation.

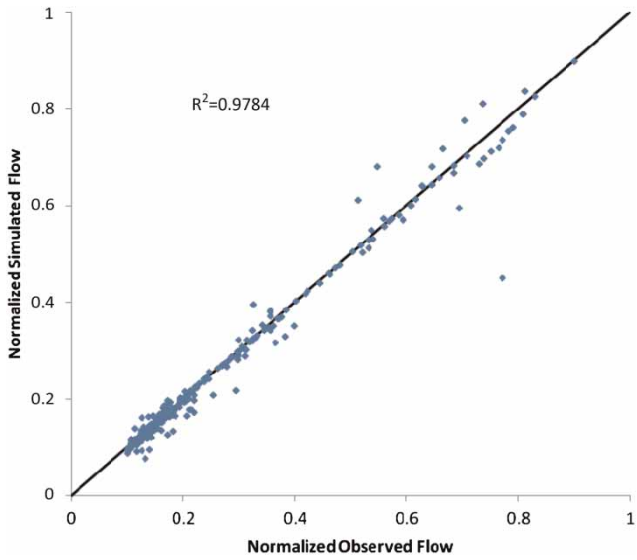

Figure 5 | Comparison between normalized simulated and normalized observed flows.

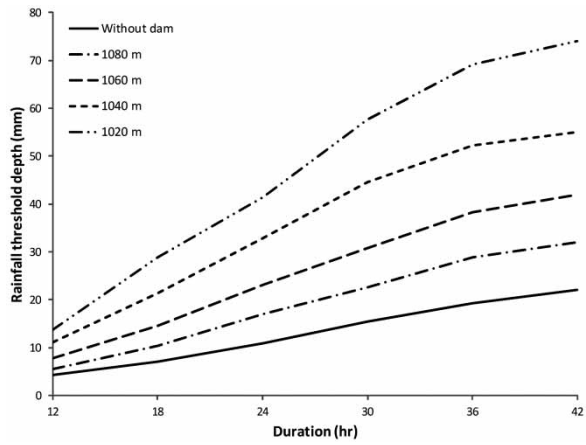

Figure 8 | RT curves with 90% probability corresponding to different initial water elevations.

that for a given rainfall duration, the RT values increase as the reservoir initial water elevation decreases.

As Figure 9 shows, the dam with a reservoir initial water elevation of 1,080 m could not hinder the devastating flood of November 30, 2000. In the case of no-dam, the flood would have reached the target location after 16 hours, while even a filled dam with water elevation of 1,080 m postpones the arrival of the peak flood for approximately 1 day. To keep the target location safe against flooding, the reservoir water level should be lower than 1,060 m.

On March 24, 2000, the dam with an initial water level of 1,060 m or higher could not prevent the occurrence of critical flow at the target location (Figure 10). The safe operation of the dam requires releasing the reservoir volume to reach the level of 1,040 m or lower. To be more conservative, dam operators may opt to use RTs with occurrence probability of 50%. If so, the reservoir should be released to reach a water elevation of less than 1,020 m (Figure 11).

The main advantage of the derived RT curves is their potential as a managerial tool in the case of heavy storms. For example, for the initial water elevation of 1,060 m, the application of the derived curves was assessed in the case of two historical rainfall events. On February 4, 2007, the first intersection between cumulative rainfall curve and 1,080 m RT curve would occur after about 13 hours from the onset of rainfall (Figure 12). Thus, the dam operator

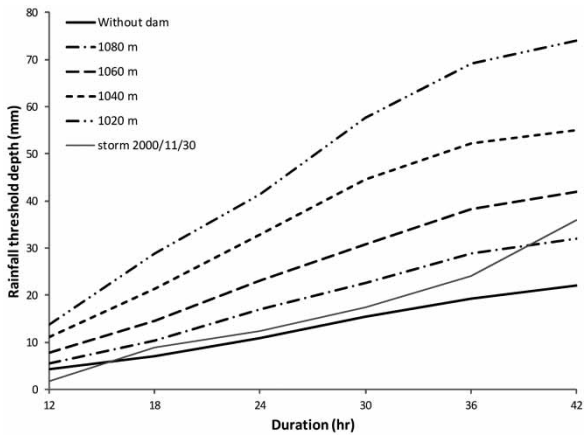

Figure 9 | Cumulative rainfall depth of November 30, 2000 flood crossing the 90% RT curves.

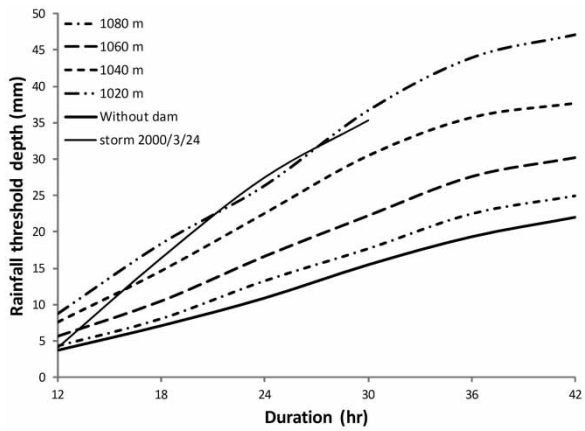

Figure 11 | Cumulative rainfall depth of March 24, 2000 flood crossing the 50% RT curves.

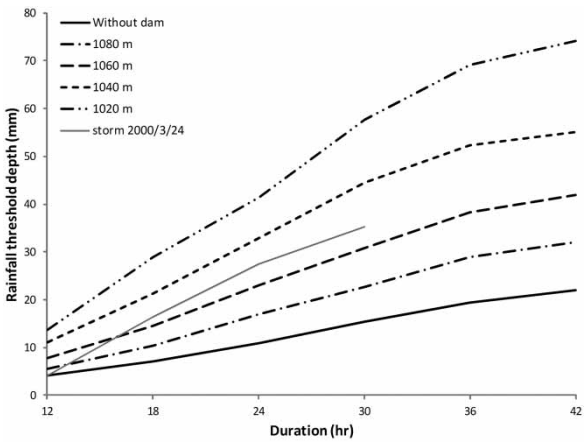

Figure 10 | Cumulative rainfall depth of March 24, 2000 flood crossing the 90% RT curves.

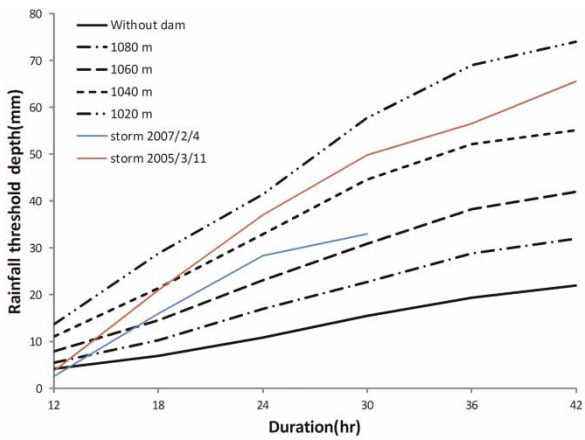

Figure 12 | Cumulative rainfall depth of February 4, 2007 and March 11, 2005 floods crossing the 50% RT curves.

may decide to release some 867 MCM to reach the 1,040 m water level. Fortunately, the slow rise of the cumulative rainfall depth assures safe flood passage through the target location. However, for the March 11, 2005, flood event, after releasing the reservoir to reach the 1,040 m level, the cumulative rainfall curve meets the RT curve and the operator must release another 635 MCM of water to lower the water elevation for another 20 m. After 24 hours, the slow rise of the cumulative rainfall curve will not cross the RT curve corresponding to 1,020 m level and flood safety is assured. Keeping the water to higher than say 1,030 m in the reservoir would have generated flooding downstream of the dam.

CONCLUSIONS

In this paper, RT curves corresponding to flooding at the target locations downstream of dams were derived for easy operation of the reservoirs under flood conditions. The strategy adopted for this purpose was an iterative loop consisting of a neural network model to simulate R-R transformation in the basin of the dam and a reservoir routing model to route the flood hydrograph through the reservoir. For the sake of taking the uncertainty of rainfall spatial distribution into account, the Monte Carlo simulation approach was used to generate a series of dimensionless random rainfall depths on the basis of observed rainfall spatial patterns. Through an iterative procedure, the basin average RTs that produce flooding conditions at the target location were determined as a function of reservoir initial water elevation. The applicability of the RT curves extracted with different probability of occurrence was demonstrated using a number of historical flood events.

An important issue in real-time application of the proposed approach is that the dam operator must select an appropriate threshold curve out of the set of extracted curves based on a given probability. A risk adverse operator, for instance, might choose the 10% probability curve corresponding to the initial reservoir water elevation prior to the flood event, particularly if an extreme flood is expected. Under normal operations, however, the 50% curve may be recommended. Based on the initial water elevation, the dam operator follows the storm progress on the cumulative rainfall curve until it crosses the selected curve. They can then start releasing the reservoir water until it reaches the next lower initial elevation and further keep track of storm development. In the case that a near real-time rainfall forecasting system is available, the lead time could increase and reservoir operation would have a better chance of succeeding in time. Also, the following conclusions are thus inferred:

- Based on the CSI criterion, the 90% RT curve was more accurate to forecast the critical discharge at the target location compared with other probabilities. Analyzing the contingency table indicated that some 10 and 50% RT curves under-estimated flood occurrence and led to increased rate of false alarms. When the cumulative rainfall curve meets a single RT curve at two points, the latter intersection is a false alarm while the former is a hit.
- Derived RT curves for different initial reservoir water elevations provide a managerial tool for real-time operation of dam reservoirs, especially in the case of expected major flooding downstream. Using real-time cumulative basin average rainfall values and the derived RT curves, the dam operator could decide how much water should be released to attain a safe water elevation in the reservoir that assures no flooding downstream.

REFERENCES

Amadio, P., Mancini, M., Menduni, G., Rabuffetti, D. & Ravazzani, G. 2003 A real-time flood forecasting system based on rainfall thresholds working on the Arno Watershed: definition and reliability analysis. In: *Proceedings of the 5th EGS Plinius Conference*, 1–3 October, Ajaccio, Corsica, France.

Coulibaly, P., Anctil, F. & Bobee, B. 2000 Daily reservoir inflow forecasting using artificial neural networks with stopped training approach. *J. Hydrol.* **230**, 244–257.

Dawson, C. W. & Wilby, R. 1998 An artificial neural network approach to rainfall-runoff modelling. *Hydrol. Sci. J.* **43** (1), 47–66.

Georgakakos, K. P. 1995 Real time prediction for flood warning and management. U.S.-Italy Research Workshop on the Hydrometeorology, Impacts, and Management of Extreme Floods Perugia (Italy), November 1995.

Giustolisi, O. & Laucelli, D. 2005 Improving generalization of artificial neural networks in rainfall-runoff modelling. *Hydrol. Sci. J.* **50** (3), 439–457.

Golian, S., Saghafian, B. & Maknoon, R. 2010 Derivation of probabilistic thresholds of spatially distributed rainfall for flood forecasting. *Water Resour. Manage.* **24**, 3547–3559.

Golian, S., Saghafian, B., Elmi, M. & Maknoon, R. 2011 Probabilistic rainfall thresholds for flood forecasting: evaluating different methodologies for modelling rainfall spatial correlation (or dependence). *Hydrol. Process.* **25** (13), 2046–2055.

Hall, M. J. & Minns, A. W. 1993 Rainfall-runoff modelling as a problem in artificial intelligence: experience with a neural network. In: *Proceedings 4th National Hydrology Symposium*, British Hydrological Society, September 1993, Cardiff, pp. 5.51–5.57.

Haykin, S. 1999 *Neural Networks: A Comprehensive Foundation*, 2nd edn. Prentice Hall, Upper Saddle River, NJ, USA.

Jain, A. & Srinivasulu, S. 2006 Integrated approach to model decomposed flow hydrograph using artificial neural network and conceptual techniques. *J. Hydrol.* **317**, 291–306.

Linsley, R. K., Franzini, J. B., Freyberg, D. L. & Techobanoglous, G. 1992 *Water Resources Engineering*. McGraw-Hill, New York.

Luino, F., Nigrelli, G., Chiarle, M., Biddoccu, M. & Cirio, C. G. 2012 A model for simulating event scenarios and estimating expected economic losses for residential buildings: preliminary results. In: *Flood Risk Assessment and Management* (S. Mambretti, ed.). WIT Press, Southampton, UK, pp. 115–125.

Martelloni, G., Segoni, S., Fanti, R. & Catani, F. 2012 Rainfall thresholds for the forecasting of landslide occurrence at regional scale. *Landslides* **9**, 485–495.

Martina, M. L. V., Todini, E. & Libralon, A. 2006 A Bayesian decision approach to rainfall thresholds based flood warning. *Hydrol. Earth Syst. Sci.* **10**, 413–426.

Mason, S. J. & Graham, N. E. 1999 Conditional probabilities, relative operating characteristics, and relative operating levels. *Weather Forecast.* **14**, 713–725.

Montesarchio, V., Lombardo, F. & Napolitano, F. 2009 Rainfall thresholds and flood warning: an operative case study. *Nat. Hazards Earth Syst. Sci.* **9**, 135–144.

Neary, D. G. & Swift, L. W. 1987 Rainfall thresholds for triggering a debris avalanching event in the southern Appalachian mountains. Debris flows-avalanches processes, recognition and mitigation. *Rev. Eng. Geol.* **7**, 81–92.

Norbiato, D., Borga, M., Esposti, S. D., Gaume, E. & Anquetin, S. 2008 Flash flood warning based on rainfall thresholds and soil moisture conditions: an assessment for gauged and ungauged basins. *J. Hydrol.* **362**, 274–290.

Norbiato, D., Borga, M. & Dinale, R. 2009 Flash flood warning in ungauged basins by use of the flash flood guidance and model-based runoff thresholds. *Meteorol. Appl.* **16**, 65–75.

Ntelekos, A. A., Goergakakos, K. P. & Krajewski, W. F. 2006 On the uncertainties of flash flood guidance: towards probabilistic forecasting of flash floods. *J. Hydrometeorol.* **7** (5), 896–915.

Rajurkar, M. P., Kothyari, U. C. & Chaube, U. C. 2002 Artificial neural networks for daily rainfall-runoff modelling. *Hydrol. Sci. J.* **47** (6), 865–877.

Rumelhart, D. E., Hinton, G. E., Williams, R. J. 1986 Learning internal representations by error propagation. In: *Paralled Distributed Processing. Explorations in the Microstructure of Cognition. Volume 1: Foundations* (D. E. Rumelhart & J. L. McClelland & the PDP Research Group, eds). MIT Press, Cambridge, MA, USA, pp. 318–362.

Saghafian, B., Anvari, S. & Morid, S. 2013 Effect of Southern Oscillation Index and spatially distributed climate data on improving the accuracy of ANN, ANFIS and K-NN streamflow forecasting models. *Expert Syst.* **30** (4), 367–380.

Saliha, A. H., Awulachew, S. B., Cullmann, J. & Horlacher, H.-B. 2011 Estimation of flow in ungauged catchments by coupling a hydrological model and neural networks: case study. *Hydrol. Res.* **42** (5), 386–400.

UNEP 2002 Early warning, forecasting and operational flood risk monitoring in Asia (Bangladesh, China and India). A Technical Report of Project (GT/1010-00-04), Division of Early Warning and Assessment (DEWA), United Nations Environment Programme (UNEP), Nairobi, Kenya.

United States Department of the Interior, Bureau of Reclamation 1974 *Design of Small Dams*. Oxford & IBH Publishing Co, New Delhi.

Vatanfada, J. 2001 Investigation of flood conditions in Iran: problems and challenges. First National Seminar on mitigate and prevent flooding, Gorgan, Iran.

Wilby, R. L., Abrahart, R. J. & Dawson, C. W. 2003 Detection of conceptual model rainfall-runoff processes inside an artificial neural network. *Hydrol. Sci. J.* **48** (2), 163–181.

Zhang, B. & Govindaraju, R. S. 2003 Geomorphology-based artificial neural networks for estimation of direct runoff over watersheds. *J. Hydrol.* **273**, 18–34.

First received 2 March 2013; accepted in revised form 6 August 2013. Available online 17 September 2013